

Heat treatment analysis of ASTM A106 steel spheroidization and erosive wear at high temperatures

<http://dx.doi.org/10.1590/0370-44672019730172>

Gabrieli Borges Ugioni Felipe^{1,5}

<https://orcid.org/0000-0001-5713-6927>

Eduardo Junca^{2,6}

<https://orcid.org/0000-0002-7068-2583>

Ângela Beatriz Coelho Arnt^{3,7}

<https://orcid.org/0000-0003-4512-0869>

Márcio Roberto da Rocha^{4,8}

<https://orcid.org/0000-0003-0904-0407>

Alexandre Gonçalves Dal-Bó^{2,9}

<https://orcid.org/0000-0002-2289-395X>

¹Universidade do Extremo Sul Catarinense - Unesc, Ciência e Engenharia de Materiais, Criciúma - Santa Catarina - Brasil.

²Universidade do Extremo Sul Catarinense - Unesc, Programa de Pós-Graduação em Ciência e Engenharia de Materiais, Criciúma - Santa Catarina - Brasil.

³Universidade do Extremo Sul Catarinense - Unesc, Departamento de Engenharia de Materiais, Criciúma - Santa Catarina - Brasil.

⁴Universidade Federal de Santa Catarina - UFSC, Coordenadoria Especial de Engenharia de Materiais, Departamento Engenharia de Materiais, Blumenau - Santa Catarina - Brasil.

E-mails: ⁵gabrieli_ugioni@hotmail.com,

⁶eduardojunca@unesc.net, ⁷anb@unesc.net,

⁸marcio.rocha@ufsc.br, ⁹adalbo@unesc.net

Abstract

The microstructures of steels are altered when exposed to high working temperatures for long periods, which results in varied physical and chemical properties. This study evaluates the erosive wear behavior of ASTM A106 steel after it is exposed to high temperatures for long durations. Samples of normalized ASTM A106GrB steel were placed in a muffle furnace at 530 and 630 °C for 50, 100, and 200 h. The erosive wear test was conducted at a speed of 20 m/s for 30 min at 450 °C with an incidence angle of 30°. Irregular alumina was used as the erodent material. The surface characterization was performed using scanning electron microscopy to determine the distribution homogeneity, morphological conditions, quantity, and spheroidization degree of the carbides. The erosive wear test results indicated that there was no volume loss after 50 h of heat treatment at 530 °C. The maximum spheroidization degree was 0.71 after 200 h at 630 °C, which decreased the hardness from 220 to 140 HV. Additionally, the volume loss reached 2.52 cm³. Therefore, the use of the ASTM A106GrB steel at working temperatures higher than 530 °C for more than 50 h decreased the mechanical behavior and the wear resistance, thereby decreasing the lifetime of the system.

Keywords: erosive wear, ASTM A106GrB steel, boiler pipes.

1. Introduction

Erosive wear, which is one of the main causes of material degradation, is caused by the contact of erodent

particles on the surface of the material (Shi *et al.*, 2018). Zaragoza-Granados *et al.* (2019) reported that components

of turbines, walls of gas turbines, and pipes are affected by erosive wear. Several authors have mentioned that

erosive wear is dependent on the operational conditions, erodent particles, and material factors (Huang, 2017; Desale *et al.*, 2008; Huang *et al.*, 2010; Parsi *et al.*, 2017; Ukpai *et al.*, 2013; and Jafari *et al.*, 2018). Therefore, the properties of the materials that are used in pipes influence the erosive wear. Okonkwo *et al.* (2016) demonstrated that the microstructure of steel is elemental in the growth of cracks, which were observed on eroded steel surfaces.

ASTM A106 is a medium carbon steel that has been extensively used in boiler pipes in thermoelectric plants at working temperatures of approximately 530 °C. However, Manssor and Ejaz (2009) indicated that in some extreme cases, the working temperature

reached 710 °C. Additionally, erodent particles that are transported in pipes consist of silicon oxide and iron oxide, which contributes to erosive wear and premature pipe failure (Manssor, 2009). Steels can also be damaged by corrosion caused by exposure to carbon dioxide (CO₂) (Trausmuth *et al.*, 2015). Therefore, heat exchange failure, which is caused by solid particles, is a challenge in the oil and gas industry. However, techniques that can be used to predict this failure are still developing. According to Gao (2017), the exposure of steel to high temperatures for long durations increases the degradation owing to microstructural changes. Several studies have reported the wear rate of steel microstructures

(Shi *et al.*, 2018; Zhang *et al.*, 2016; and Stack, 2011). However, a thorough search of the relevant literature yielded no study that shows the correlation between spheroidization and erosive wear in ASTM A106 steel.

Spheroidization occurs in steels that are exposed to high temperatures for long isothermal durations (Amos *et al.*, 2018). Spheroidal steels exhibit sufficient strength and ductility even when reduced hardness is observed, which is essential in cold forming (Zheng *et al.*, 2017; Lee *et al.*, 2013). Therefore, this study investigates the erosive wear of ASTM A106 steel under different conditions of spheroidized heat treatment to correlate microstructure and performance.

2. Experiment

The tests were conducted using a 3.91 mm thick hot-rolled ASTM A 106 grade B

seamless steel pipe with a 50.8 mm diameter. Table 1 summarizes the chemical com-

position of the steel that was determined by a Spectrolab optical emission spectrometer.

Table 1 - Chemical composition of the ASTM A106GrB steel.

C	Mn	P	S	Si	Ni	Cr	Mo	Cu
0.19	0.43	0.17	0.12	0.21	0.0067	0.20	0.1	0.4

The steel was normalized at 900 °C for 1 h (without a protective atmosphere) to remove residual stresses and distortions. Thereafter, a steel surface thickness of 1 mm was removed to eliminate possible areas of oxidation and decarburization that may have formed during the heat treatment. The samples were sanded and polished (alumina 1 μm), followed by the microstructure of the normalized steel being exposed using a 3% nital solution. Images were obtained using an Olympus

BX41RF/LED optical microscope and a Zeiss EVO-MA10 scanning electron microscope (SEM). The normalized steel was placed in the muffle furnace to allow for the spheroidizing heat treatment at 530 and 630 °C for 50, 100, and 200 h. The heat treatment of spheroidization occurred without a controlled atmosphere. The spheroidized steel was cleaned using ethyl alcohol and dried using air. This was performed to determine the initial mass of the sample using a Mettler analytical balance.

The erosive wear test was conducted using 30 mm diameter samples following the ASTM G-76 standard. The erodent material (alumina) with irregular morphology was fluxed on the surface of the sample at 20 m/s and 450 °C for 30 min. Three samples were used for each heat treatment experiment. The incidence angle was 30° (Zhang *et al.*, 2016; Zhang, 2016). Table 2 shows the size analysis that was conducted on the erodent material using laser diffraction.

Table 2 - Size analysis of the alumina that was used as erodent material in wear tests.

D_{10} (μm)	D_{50} (μm)	D_{90} (μm)
171.57	375.54	571.39

Each sample was cleaned with ethyl alcohol and dried using air to obtain the

final mass after the erosive wear test. The volume loss was calculated using Equation 1:

$$\text{Volume loss} = \frac{m_i - m_f}{7.86} \times 100 \quad (\text{Equation 1})$$

where m_i is the mass of the sample before the erosion test, m_f is the mass of the sample after the erosion test, and 7.86 is the iron density (g/cm³).

The surface characterization of

each specimen was analyzed using an Olympus optical microscope (model SZ61) to verify the distribution of the carbides and grain size of the steel. The morphology, quantity, and the

degree of spheroidization of the carbides were analyzed using SEM. The carbide quantification was determined using ImageJ software.

3. Results and discussion

3.1 Heat treatment

Figure 1 shows that ferrite and perlite are the main phases present in the normalized ASTM A106GrB steel.

Figure 2a shows that the car-

bide spheroidization started within 50 h at 530 °C. When the time of the heat treatment was increased to 100 h, the number of carbides that were

spheroidized increased (Fig 2b). Carbides coalesced after 200 h of heat treatment at 530 °C (Fig 2c).

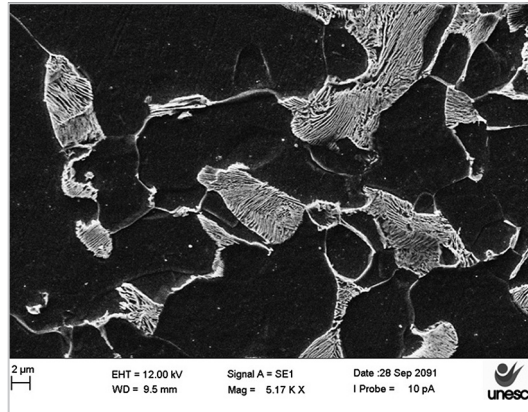


Figure 1 - Scanning electron microscopy image of the normalized ASTM A106GrB steel.

Table 3 shows that 523 and 555 carbides/mm² were spheroidized, respectively. This suggests that the fragmentation of the perlite occurred under these conditions. Additionally, the number of carbides decreased to 431 carbides/mm² and the carbide size increased to 0.40 μm during 200 h of heat treatment at 530 °C.

Fragmentation of the perlite occurred up to 50 h into the treatment when using a 630 °C heat treatment during spheroidization (Figure 3a). Fig 3b and 3c show that a reduction in the number of carbides occurred as the heat treatment time increased. Table 3 shows the carbide sizes of 0.48 and 0.52 μm for 100 and 200 h

of heat treatment, respectively. The results demonstrate that when the heat treatment temperature increased from 530 to 630 °C, the carbide size increased from 0.4 to 0.52 μm. In addition, the spheroidization degree increased. Subsequently, the circularity of the carbides (from 0.56 to 0.71) is demonstrated.

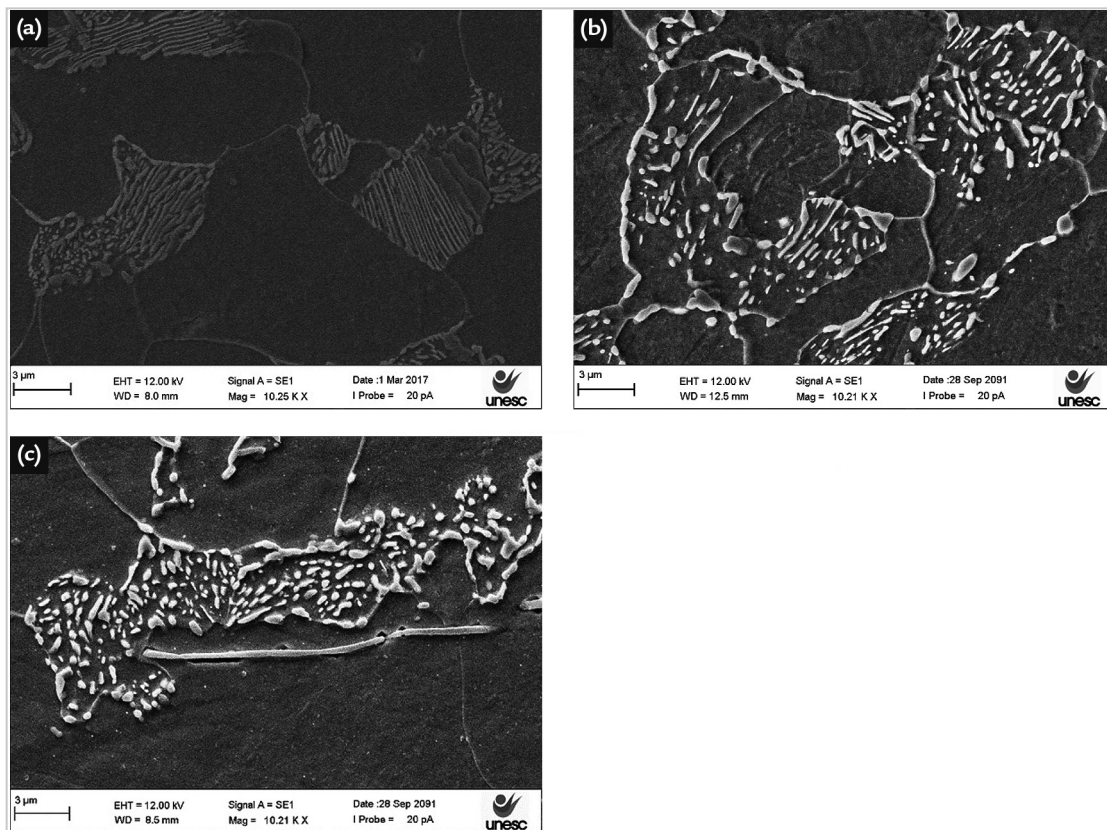


Figure 2 - Microstructural evolution during the spheroidizing heat treatment of the ASTM A106GrB steel at 530 °C. a) 50 h; b) 100 h; c) 200 h.

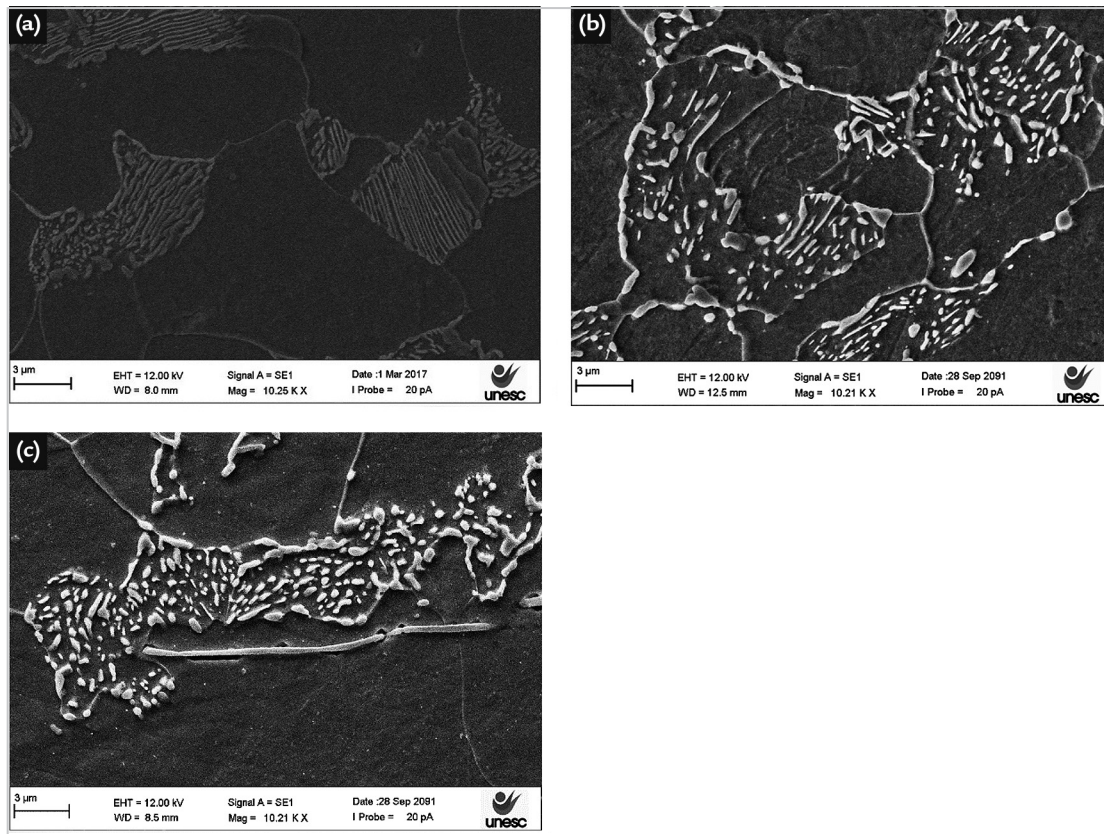


Figure 3 - Microstructural evolution during the spheroidizing heat treatment of the ASTM A106GrB steel at 630 °C. a) 50 h; b) 100 h; c) 200 h.

Table 3 - Spheroidization degree, carbide size, and the number of carbides obtained during the spheroidizing heat treatment of the ASTM A106GrB steel at 530 and 630 °C.

Temperature	Time	Spheroidization degree (0–1)	Carbide size (μm)	Number of carbide/mm ²
Normalized steel		-	0.62	507
530°C	50h	0.40	0.59	523
	100h	0.52	0.20	555
	200h	0.56	0.40	431
630°C	50h	0.62	0.38	329
	100h	0.65	0.48	302
	200h	0.71	0.52	277

Figure 4a shows the variation in the hardness of the ASTM A106GrB steel for different heat treatment conditions (i.e., temperature and time) during spheroidi-

zation. Fig 4b shows the relationship between the carbide particles and steel hardness. Hardness values of 145 and 165 HV were obtained for 50 h at 530

and 630 °C, respectively. Table 3 shows a decrease in the number of carbide particles to 523 and 431 particles/mm² at 530 and 630 °C for 50 h, respectively.

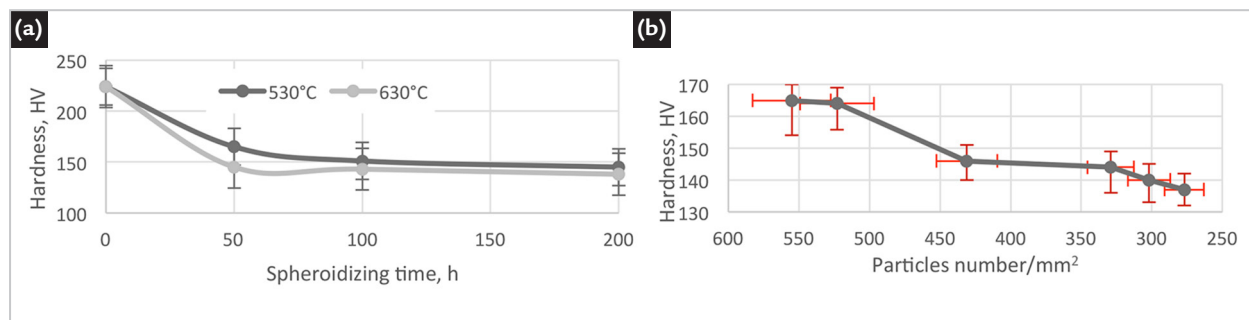


Figure 4 - a) Influence of heat treatment on the steel hardness; b) influence of the number of particles on steel hardness.

A non-linear relationship between carbide particles and hardness was observed. Furthermore, when the heat treatment time was increased during spheroidization, the steel morphology and number of carbide particles changed, which indicated that steel hardness reduces when heat treatment for less than 50 h. According to Karadeniz (2008), particle coalescence occurs slowly in the final stages after the initial

spheroidization steps, which contributes to a slow decrease in the hardness at the final stage of spheroidization.

Figure 5 shows the relationship between ferritic grain size and duration of heat treatment. The heat treatment at 630 °C for 200 h produced a larger final grain size because using a higher temperature benefited the carbon diffusion process (Pawlak, 2016). However, when the growth rate of the

ferritic grains increased, the carbide number decreased. This is because the lower number of carbides that block grain boundary growth (Islam, 2017), reduce the mechanical strength of steel. Additionally, the error bars show that there is only a statistical difference for 200 h of heat treatment. The fragmentation of the carbides and coalescence occurred during 50 and 100 h of heat treatment.

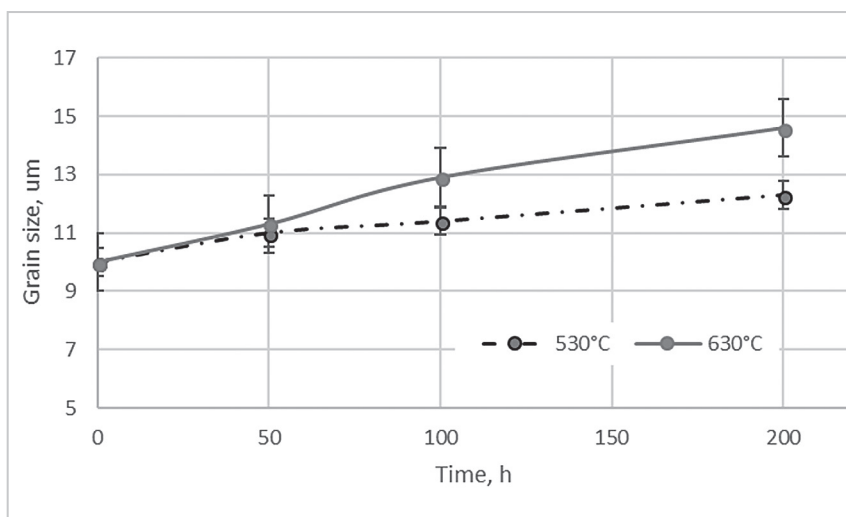


Figure 5 - Evaluation of the heat treatment temperature on the ferritic grain size.

Figure 6 displays steel microstructure images obtained using optical microscopy at different heat treatment times and temperatures. There was no

change in the steel microstructures for the 530 °C heat treatment. However, when the heat treatment temperature was increased to 630 °C, the carbide

particles fragmented in 50 h (Fig 6d). Additionally, Fig 6e shows that the steel microstructure is perlite with spheroidal carbides.

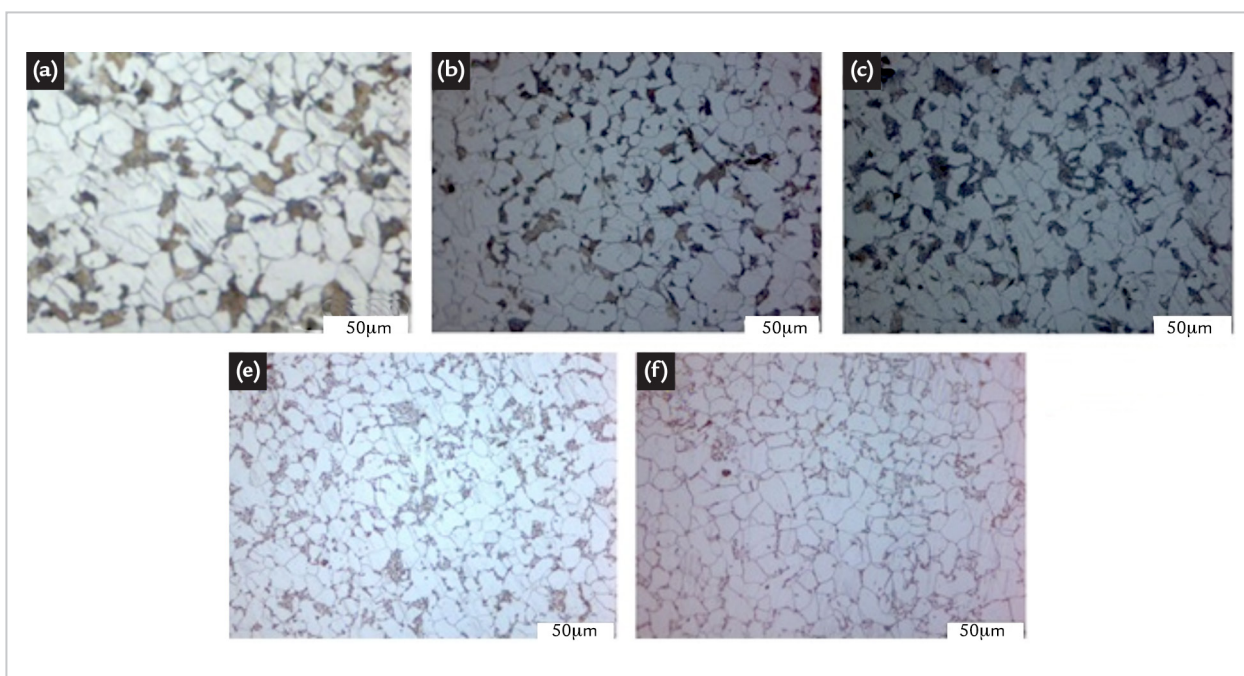


Figure 6 - a) Normalized microstructure of the ASTM A106GrB steel; heat treatment at b) 530 °C for 50 h; c) 530 °C for 200 h; d) 630 °C for 50 h; and e) 630 °C for 200 h.

3.2 Erosion test

Figure 7a displays volume loss versus time of the heat treatment during spheroidization. When the duration and temperature were increased during spheroidization, the wear rate increased. The heat treatment at 530 °C for 200 h achieved a spheroidization degree of 0.56 and a volume loss of 2 cm³. However,

the heat treatment at 630 °C for 200 h achieved a spheroidization degree of 0.71 and a volume loss of 2.52 cm³. The largest volume loss was related to the heat treatment over a longer time and at a higher temperature (630 °C and 200 h). Fig 7b shows the volume loss versus the number of carbides in the

spheroidized steels. Higher volume losses occurred in the samples that had fewer carbide particles. Therefore, the heat treatment performed over a longer time and at a higher temperature increased the coalescence and diffusion of carbon, which reduced the number of carbides and steel hardness.

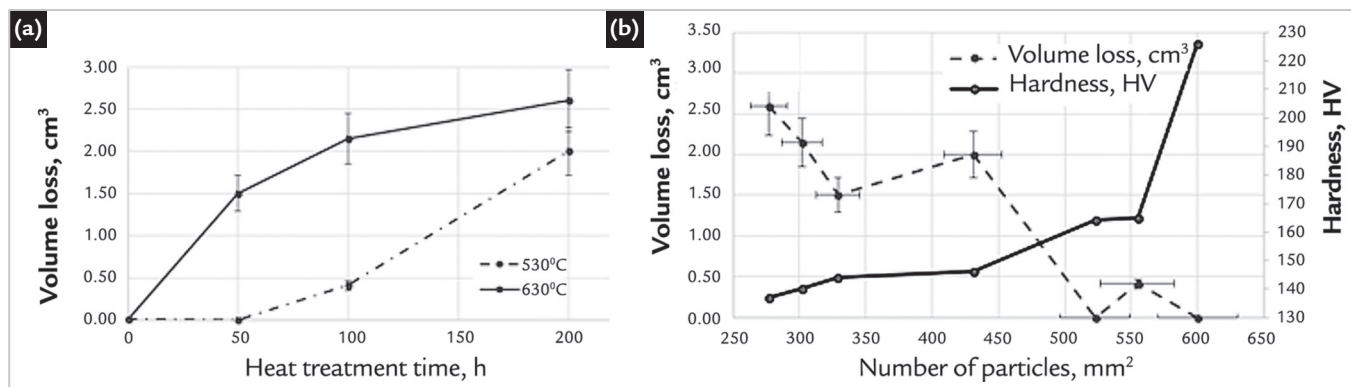


Figure 7 - Evaluation of a) the temperature and time on the volume loss; b) the number of particles on the volume loss and steel hardness at 530 and 630 °C for 50, 100, and 200 h.

Fig 7a also demonstrates that the highest erosive wear resistance occurred during the initial stage (normalized steel). The wear process

increased from the beginning of the heat treatment during spheroidization and caused a decreased of the hardness from 226 to 165 HV. According to

Javaheri *et al.* (2018), the loss of hardness involves the initial steps of perlite lamellae fragmentation and cementite particle spheroidization.

3.3 Surface characterization

Figure 8 shows the SEM images of the sample surfaces before and after the erosion tests. The normalized steel (Fig 8a) showed no scratches or craters on the surface, which verifies the absence of

mass loss due to the erosion test. However, Fig 8b and 8c show that the samples that were subjected to the heat treatment during spheroidization had several scratches or craters on the surface. Additionally,

plastic deformation was detected on the surface. According to Hong *et al.* (2015), the increase in heat treatment temperature decreases the erosion resistance because of the increase in the steel grain size.

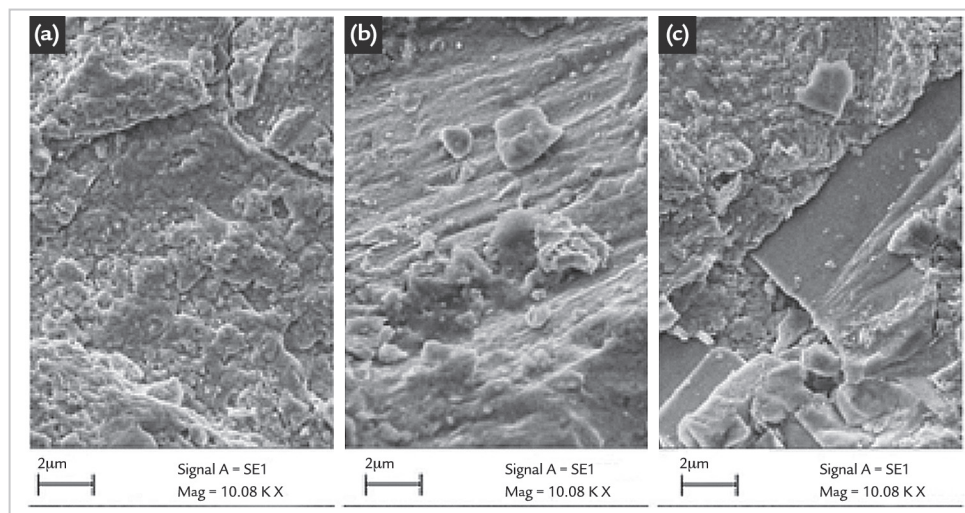


Figure 8 - Image of the steel surfaces after the erosion tests. a) Normalized steel; b) 630 °C for 100 h; c) 630 °C for 200 h.

The heat treatment during spheroidization at 630 °C for 100 h (Fig. 8c) shows the largest uneven surface owing to lower material hardness. A similar result was obtained by Alam

and Farhat (2018). The authors said that crater formation occurred because of the penetration of the deep erodent particle in the steel. The removal of the erodent particles on the surface results

in craters and vulnerable lips. This type of behavior was also observed by Zhang *et al.*, 2016.

According to Rosa *et al.* (2017), the wear process begins with flake for-

mation on the surface, followed by the deformation of the surrounding regions

owing to the impact of erodent particles. Samples with low spheroidization

levels (i.e., greater hardness) showed microcracks on the surface.

4. Conclusions

The normalized ASTM A106GrB steel consisted of perlite and ferrite with a hardness of 226 HV. Subjecting steel to temperatures of 530 and 630 °C resulted in the spheroidization of the carbides after 50 h of heat treatment. Maximum hardness loss rates from 226 to 165 and 145 HV at 530 and 630 °C, respectively, were

observed. No volume loss was observed for the heat treatment at 530 °C for 50 h. However, when exposing the sample to 630 °C for 50 h, a 1.5 cm³ and 3.0 cm³/h volume loss and volume loss rate were observed, respectively. The exposure of the ASTM A106GrB steel to 630 °C for 200 h increased the volume loss rate to

5.04 cm³/h because of the higher number of spheroidized carbides. Therefore, the use of ASTM A106GrB steel at temperatures higher than 530 °C for long periods (above 50 h) can negatively impact the mechanical behavior and decrease wear resistance, thereby decreasing the lifetime of the system.

References

- ALAM, T.; FARHAT, Z. N. Slurry erosion surface damage under normal impact for pipeline steels. *Engineering Failure Analysis*, v. 90, p. 116-128, Aug. 2018.
- CUNKUI HUANG, C.; MINEV, P.; LUO, J.; NANDAKUMAR, K. A phenomenological model for erosion of material in a horizontal slurry pipeline flow. *Wear*, v. 269, p. 190-196, Jun. 2010.
- DESALE, G.; GANDHI, B. K.; JAIN, S. C. Slurry erosion of ductile materials under normal impact condition. *Wear*, v. 264, N. 3-4, p. 322-330, Feb. 2008.
- GAO, W.; LI, Y.; KONG, L. Numerical investigation of erosion of tube sheet and tubes of a shell and tube heat exchanger. *Computers & Chemical Engineering*, v., 96, 4 January 2017.
- HONG, S.-M.; PARK, J.-J.; PARK, E.-K.; LEE, M.-K.; RHEE, C.-K.; LEE, J. K.; LEE, J. G.; KIM, K. H. Cavitation erosion behavior of SA 106B carbon steel after treatment of the melt with nano-sized TiC particles. *Tribology International*, v. 92, p. 585-594, Dec. 2015.
- ISLAM, A.; FARHAT, Z. Erosion-corrosion mechanism and comparison of erosion-corrosion performance of API steels. *Wear*, v. 376-377, Part A, p. 533-451, 15 Apr. 2017.
- JAFARI, A.; DEHGHANI, K.; BAHAAADDINIA, K.; HATAIE, R. A. Experimental comparison of abrasive and erosive wear characteristics of four wear-resistant steels. *Wear*, v. 416-417, p. 14-26, 2018.
- JAVAHARI, V.; PORTER, D.; KUOKKALA, V.-T. Slurry erosion of steel – Review of tests, mechanisms and materials. *Wear*, N. 408-409, p. 248-273, Aug. 2018.
- KARADENIZ, E. Influence of different initial microstructure on the process of spheroidization in cold forging. *Materials and Design*, v. 29, n. 1, p. 251-256, 2008.
- KUBENDRAN AMOS, P. G.; BHATTACHARYA, A.; NESTLER, B.; ANKIT, K. Mechanisms of pearlite spheroidization: Insights from 3D phase-field simulations. *Acta Materialia*, v. 161, p. 400-411, Dec. 2018.
- LEE, Y.-W.; SON, Y.-I.; LEE, S.-J. Microstructure and mechanical properties of spheroidized D6AC steel. *Materials Science & Engineering A*, v. 585, p. 94-99, Nov. 2013.
- MANSOR, M.; EJAZ, N. Prediction of in-service microstructural degradation of A106 steel using eddy current technique. *Materials Characterization*, v. 60, n. 12, p. 1591-1596, Dec. 2009.
- OKONKWO, P. C.; SHAKOOR, R. A.; AHMED, E.; MOHAMED, A. M. A. Erosive wear performance of API X42 pipeline steel. *Engineering Failure Analysis*, v. 60, p. 86-95, Feb. 2016.
- PARSI, M.; KARA, M.; AGRAWAL, M.; KESANA, N.; JATALE, A.; SHARMA, P.; KSHIRAZI, S. CFD simulation of sandparticle erosion under multiphase flow conditions. *Wear*, N. 376-377, p. 1176-1184, 2017.
- PAWLAK, K.; BIAŁOBRZESKA, B.; KONAT, Ł. The influence of austenitizing temperature on prior austenite grain size and resistance to abrasion wear of selected low-alloy boron steel. *Archives of Civil and Mechanical Engineering*, v. 16, n. 4, p. 913-926, Sep. 2016.
- SEDANO-DE LA ROSA, C.; VITE-TORRES, M.; GALLARDO HERNÁNDEZ, E. A.; LAGUNA-CAMACHO, J. R.; GODINEZ-SALCEDO, J. G.; FARFAN-CABRERA, L. I. Effect of tangential velocity on erosion of ASTM A-106 Grade B steel pipe under turbulent swirling impinging jet. *Tribology International*, v. 113, p. 500-506, Sep. 2017.
- SHARMA, A.; KUMAR, A.; TYAGI, R. Erosive wear analysis of medium carbon dual phase steel under dry ambient condition. *Wear*, v. 334-335, p. 91-98, Jul. 2015.
- SHI, J.; CHEN, H.; JIA, S.; WANG, W. Rapid and low-cost fabrication of thermoelectric composite using low-pressure cold pressing and thermocuring methods. *Materials Letters*, v. 212, p. 299-302, Feb. 2018.
- STACK, M. M.; ABDULRAHMAN, G. H. Mapping erosion-corrosion of carbon steel in oil-water solutions: effects of velocity and applied potential. *Wear*, v. 274-275, p. 401-413, Jan. 2011.
- TRAUSMUTH, A.; RODRIGUEZ RIPOLI, M.; ZEHETHOFER, G.; VOGL, T.; BADISCH, E. Impact of corrosion on sliding wear properties of low-alloyed carbon steel. *Wear*, v. 328-329, p. 338-347, Apr. 2015.
- UKPAI, J. I.; BARKER, R.; HU, X.; NEVILLE, A. Determination of particle impacts and impact energy in the erosion

- of X65 carbon steel using acoustic emission technique. *Tribology International*, n. 65, p. 161–170, 2013.
- ZARAGOZA-GRANADOS, J.; GALLARDO-HERNÁNDEZ, E. A.; VITE-TORRES, M.; SEDANO-DE LA ROSA, C. Erosion behaviour of AISI 310 stainless steel at 450 °C under turbulent swirling impinging jets. *Wear*, v. 426-427, Part A, p. 637-642, Apr. 2019.
- ZHANG, J.; KANG, J.; FAN, J.; GAO, J. Research on erosion wear of high-pressure pipes during hydraulic fracturing slurry flow. *Journal of Loss Prevention in the Process Industries*, v. 43, p. 438-448, Sep. 2016.
- ZHANG, J.; KANG, J.; FAN, J.; GAO, J. Study on erosion wear of fracturing pipeline under the action of multiphase flow in oil & gas industry. *Journal of Natural Gas Science and Engineering*, v. 32, p. 334-346, May 2016.
- ZHENG, C.; LIU, Y.; CHEN, C.; QIN, J.; JI, R.; CAI, B. Numerical study of impact erosion of multiple solid particle. *Applied Surface Science*, v. 423, p. 176-184, Nov. 2017.

Received: 6 January 2020 - Accepted: 20 July 2020.